

THE ROLE OF SURFACE TENSION AND MOBILITY MODEL IN SIMULATIONS OF GRAIN GROWTH

TIAGO SALVADOR AND SELIM ESEDOĞLU

ABSTRACT. We explore the effects of surface tension and mobility models in simulations of grain growth using threshold dynamics algorithms that allow performing large scale simulations, while naturally capturing the Herring angle condition at junctions and automatically handling topological transitions. The results indicate that in two dimensions, the different surface tension / mobility models considered do not play a significant role in the stationary grain size distribution. However, in three dimensions, there is a substantial difference between the distributions obtained from the same three models, depending on whether the reduced mobilities are isotropic or anisotropic. Additional results show that in three dimensions, the misorientation distribution function of a grain network with random orientation texture returns to the close vicinity of the Mackenzie distribution even if started very far from it.

CONTENTS

1. Introduction	1
2. Previous Work	3
3. Our model and algorithm	4
4. Large scale simulations	7
5. Conclusions	15
6. Acknowledgements	17
References	17

1. INTRODUCTION

The shapes and sizes of grains constituting polycrystalline materials, such as most metals and ceramics, influence important physical attributes of these materials, for example their conductivity and yield strength. Therefore, there has been much interest in modeling and simulation of grain boundary motion during common manufacturing processes, such as annealing. In particular, the evolution of grain size distribution (GSD), the grain boundary character distribution (GBCD), as well as a simpler version of the latter, the misorientation distribution function (MDF), have been a central focus of research in materials science.

In this paper, we report simulation results for grain boundary motion at the mesoscale, using a recent, very concise and flexible numerical algorithm developed for the continuum model of grain boundaries that was introduced by Mullins

Date: July 29, 2019.

Key words and phrases. grain growth, grain size distribution, misorientation distribution function, simulation, polycrystalline materials.

[Mul56] and earlier authors. According to this well known model, interfaces in the grain network evolve via steepest descent for an energy that penalizes surface areas of the interfaces, often weighted by a factor, known as the surface tension, that depends on the misorientation across each interface. The resulting dynamics is described by a system of partial differential equations (PDEs), coupled to each other along junctions by what are known as Herring angle conditions [Her99], and allows specifying in addition a mobility factor for each interface. The results we present are the first large scale simulations using the new algorithm proposed in [SE18] for this PDE system.

We investigate several questions that have repeatedly come up in previous literature concerning certain statistics of the grain network. In particular, we study, in both two and three dimensions:

- The effect of surface tension and mobility model used on statistics such as the GSD.
- The asymptotic behavior of the MDF and its dependence on initial configuration.

Specifically, we simulate in both 2D and 3D Mullins’ mesoscale model with

- (i) Read-Shockley surface tensions [RS50] (and its extension [HHM01] to 3D anisotropy) along with isotropic mobilities,
- (ii) Read-Shockley surface tensions with “reciprocal” mobilities resulting in isotropic *reduced* mobilities but asymmetric junction angles, and
- (iii) Isotropic surface tensions and mobilities, resulting in isotropic reduced mobilities as well as symmetric (all 120°) junction angles.

We compare to experimental data whenever it is available in existing literature. Some of our results and conclusions differ substantially from earlier studies. Highlights of our findings are:

- In 2D simulations, the stationary GSD that is reached appears to not depend on the surface tension and mobility models used: it is essentially the same in all three surface tension / mobility combinations (i), (ii), (iii) used in our simulations. This is in agreement with a variety of previous studies, e.g. [UHK⁺02, Hal14].
- However, in 3D, the stationary GSD reached is substantially different when Read-Shockley surface tensions along with isotropic mobilities (i) are used, compared to (ii) and (iii) that result in isotropic reduced mobilities. This finding appears to be distinct from earlier studies, e.g. [GMH⁺09].
- Moreover, the different GSD reached in 3D by models (i) and (ii) that differ only in their choice of mobilities constitutes a contrary point to previous studies that suggest mobilities do not play a significant role in the long time behavior of the GSD.
- The GSD reached by (ii) and (iii) are almost identical in both 2D and 3D, even though junction angles in these simulations are very different, suggesting that perhaps the isotropy vs. anisotropy of reduced mobilities is what is significant.
- The GSD reached in our 3D simulations with surface tension / mobility combination (i) is not less consistent with experimental measurements [RLS10, ZSIE04, GHU⁺06], which have substantial variation themselves.

- Statistics of grain *shapes*, such as that of isoperimetric ratios (eccentricities), also display considerable dependence on the choice of surface tension / mobility model.
- Models (i) & (ii) allow us to study the asymptotic behavior of the MDF. Confirming earlier studies, the two drastically different choices of mobility in (i) & (ii) lead to almost identical behavior, both in 2D and 3D. Distinct from earlier studies, we exhibit 3D initial data with MDFs perturbed substantially away from the Mackenzie distribution and observe the MDF return to a very close vicinity of the Mackenzie distribution, using either (i) or (ii) as the surface tension / mobility model.

The code for the simulations is publicly available and can be found at <https://github.com/tiagosalvador/statisticsGBM>.

2. PREVIOUS WORK

The existing literature on the statistics of grain shapes and sizes during annealing is absolutely vast, both from the experimental and the modeling and simulation side. Our discussion will therefore be necessarily limited to a few representative studies closest to the questions addressed in the present paper.

There are a plethora of numerical algorithms developed for the simulation of Mullins' mesoscale model of grain boundary motion. They include the Monte Carlo Potts, front tracking, phase field, level set, and threshold dynamics methods. In principle, all these methods should converge to the same continuum model described by the same system of PDEs, provided that various parameters appearing in them are scaled appropriately, at least until topological changes start to take place (even then, one hopes there would be agreement in the vast majority of situations). Nevertheless, there isn't always good agreement even among simulations.

Very large, well resolved simulations of normal grain growth were carried out by Mason et. al. [MLMS15] using the front tracking method in both 2D and 3D. The authors catalogue a large number of grain size and shape statistics, for the two dimensional model, for the three dimensional model, and for two dimensional slices of the three dimensional model. However, this work is restricted to the equal surface tension, equal mobility, i.e. the fully isotropic, version of Mullins' model. That in particular means the exclusion of such statistics as the GBCD or the MDF which are predicated on variation of surface tension between different interfaces in the network. Furthermore, left unaddressed is the question of how sensitively these shape and size statistics depend on the surface tension and mobility model used in conjunction with Mullins' continuum model.

Upmanyu et. al. [UHK⁺02] study the dependence of grain boundary statistics on the surface tension and mobility models used via Monte Carlo Potts and phase field simulations in 2D. The GSDs they report, including when the surface tension, the mobility, and both are anisotropic, show little deviation from that of the isotropic model; they all follow a more or less log-normal distribution. Their investigation of the MDF in the same vein reveals strong dependence on the surface tension model used, but not so much on mobilities: The network is driven towards a prevalence of interfaces with low misorientations and therefore low surface tensions. Other statistics, such as the number of neighbors (or faces), are also observed to have a much more pronounced dependence on surface tensions than mobilities. Similar

MC Potts simulations in [HHM01] also show little difference between the GSDs of isotropic vs. Read-Shockley surface tensions.

Gruber et. al. [GMH⁺09] carry out MC Potts simulations in 3D, using isotropic as well as Read-Shockley (anisotropic) surface tension models. Among the grain properties they document are the GSD and the MDF. They observe no difference between the stationary GSDs reached using isotropic vs. anisotropic surface tension models. As regards the MDF, this study suggests surface tension anisotropy has a measurable effect on the steady state MDF reached in simulations that start from an initial data with random orientation texture, regardless of the dimension. When the initial orientation texture is not random, no steady state for the MDF is observed in the case of anisotropic surface tensions: instead, a proliferation of low angle grain boundaries results in a gradual but persistent concentration of the MDF at the origin.

Kim et. al. [KKKP06] carry out phase field simulations in 2D and 3D using isotropic surface tensions and mobilities. In 3D, the stationary GSD they reach (given in terms of the reduced equivalent radii) follows very closely the Hillert distribution. On the other hand, the Monte-Carlo Potts simulations of Zoellner et. al. [ZS06] in 3D, using isotropic surface tensions and mobilities, and starting from an initial data with random texture, results in a stationary GSD that is quite far from the Hillert distribution. The more recent very large scale simulations of Miyoshi et. al. [MTO⁺17] in 3D using the phase field method also yielded a GSD similar to that of [ZS06] that deviates substantially from the Hillert distribution.

The recent 2D simulations reported in [MT17] using a phase field method treat surface tension / mobility models (i) and (iii), as well as a third model that combines Read-Shockley surface tensions with mobilities that have a sigmoidal dependence on the misorientation angle as proposed by Humphreys [Hum97]. For this third surface tension / mobility model, the stationary GSD they obtain is significantly different from those with models (i) & (iii). The stationary GSDs of models (i) & (iii) are reported to be very similar.

3. OUR MODEL AND ALGORITHM

Our starting point is the curvature driven grain boundary motion model that goes back at least to Mullins [Mul56]. According to this model, grain boundaries evolve via steepest descent for the energy

$$(1) \quad E = \sum_{i < j} \sigma_{ij} \text{Area}(\Gamma_{ij})$$

where $\Gamma_{i,j}$ denotes the boundary between two adjacent grains Σ_i and Σ_j . In particular we will neglect the normal dependence of the energy density, but allow each grain boundary $\Gamma_{i,j}$ to have a distinct surface tension $\sigma_{i,j}$. The very special case $\sigma_{i,j} = 1$ for all $i \neq j$ is often referred to as the *isotropic* surface tension model. We will also be interested in the surface tension model due to Read & Shockley [RS50] and its extension [HHM01] to 3D crystallography:

$$(2) \quad \sigma_{ij} = \begin{cases} \frac{\theta_{ij}}{\theta_*} \left(1 - \log \left(\frac{\theta_{ij}}{\theta_*} \right) \right) & \text{if } \theta_{ij} \in [0, \theta_*], \\ 1 & \text{if } \theta_{ij} \geq \theta_*. \end{cases}$$

where $\theta_{i,j}$ is the misorientation angle between Σ_i and Σ_j and θ_* is the Brandon angle [Bra66], often taken to be between 15° and 30°. Following the convention

in materials science literature, we will refer to (2) as an *anisotropic* surface tension model, even though there is still no dependence on the normal to the interface.

In two dimensions, each grain Σ_i is modeled as a square lattice and is assigned an orientation angle θ_i of a clockwise rotation about the origin that maps it back to the standard two-dimensional lattice \mathbb{Z}^2 . Thus, the misorientation between two grains Σ_i and Σ_j is given by

$$(3) \quad \theta_{i,j} = \min_{k \in \mathbb{Z}} \left| \theta_i - \theta_j + k \frac{\pi}{2} \right|.$$

In three dimensions, the orientation of a grain with cubic lattice can be described (nonuniquely) by a matrix $g \in SO(3)$ that corresponds to the rotation required to obtain the lattice of the grain from the standard integer lattice \mathbb{Z}^3 . The misorientation angle between two grains Σ_i and Σ_j is defined as

$$(4) \quad \theta_{i,j} = \min_{r \in \mathcal{O}} \arccos \left(\frac{1}{2} (\text{tr}(r g_i g_j^T) - 1) \right),$$

where \mathcal{O} denotes the octahedral group (of symmetries of the cube in the three dimensions).

According to Mullins, the dynamics associated with energy (1) is given by L^2 gradient descent for the interfaces, leading to the normal speed

$$(5) \quad v_{i,j} = \mu_{i,j} \sigma_{i,j} \kappa_{i,j}$$

for interface $\Gamma_{i,j}$, where $\kappa_{i,j}$ denotes the mean curvature of $\Gamma_{i,j}$ and $\mu_{i,j} > 0$ is a mobility factor. In addition, a condition known as the *Herring angle condition* [Her99] holds along triple junctions. At a junction formed by the meeting of the three distinct grains Σ_i , Σ_j and Σ_k , this condition reads

$$(6) \quad \sigma_{i,j} n_{i,j} + \sigma_{j,k} n_{j,k} + \sigma_{k,i} n_{k,i} = 0.$$

As a consequence the angles formed by normals $n_{i,j}$, $n_{j,k}$ and $n_{k,i}$ to the three interfaces $\Gamma_{i,j}$, $\Gamma_{j,k}$ and $\Gamma_{k,i}$ along the triple junction are determined by their associated surface tensions; this relation is also known as Young's law.

The algorithms used in this study are obtained from a non-local approximation to energy (1)

$$(7) \quad \frac{1}{\sqrt{\delta t}} \sum_{i < j} \sigma_{i,j} \int_{\Sigma_i} G_{\sqrt{\delta t}} * \mathbb{1}_{\Sigma_j} dx$$

where G_t denotes the Gaussian kernel

$$G_{\sqrt{t}}(x) = \frac{1}{(4\pi t)^{d/2}} \exp \left(-\frac{|x|^2}{4t} \right)$$

and $\mathbb{1}_{\Sigma}(x)$ denotes the characteristic function for a set Σ :

$$\mathbb{1}_{\Sigma}(x) = \begin{cases} 1 & \text{if } x \in \Sigma, \\ 0 & \text{otherwise.} \end{cases}$$

The width δt of the Gaussian kernel appearing in (7) ends up playing the role of the time step size for our scheme, described below, that approximates gradient descent of (1) in L^2 sense, as described by [Mul56]. Energy (7) has been proposed

in [EO15] and has been shown to converge in a very precise sense (namely, that of Gamma-convergence) to energy (1) in the limit $\delta t \rightarrow 0^+$. Intuitively, we have

$$\frac{1}{\sqrt{\delta t}} \int_{\Sigma_i} G_{\sqrt{\delta t}} * \mathbb{1}_{\Sigma_j} dx \approx \frac{1}{\sqrt{\pi}} \text{Area}(\Gamma_{i,j})$$

since the function $\frac{1}{\sqrt{\delta t}} \mathbb{1}_{\Sigma_i} G_{\sqrt{\delta t}} * \mathbb{1}_{\Sigma_j}$ approximates a delta function concentrating near $\Gamma_{i,j}$ as $\delta t \rightarrow 0^+$. The reason for our interest in this specific - perhaps unusual - approximation of Mullins' energy is that it generates exceptionally simple and efficient algorithms for simulating gradient descent dynamics associated with (1). Indeed, it has been shown in [EO15] to lead, in a systematic way, to the correct multiphase, arbitrary surface tension analogue of a very fast algorithm known as *threshold dynamics* that was originally proposed in [MBO92, MBO94] for networks with all equal surface tensions (i.e., $\theta_{i,j} = 1$ for all i and j) and mobilities.

We start by recalling Algorithm 1, the simplest version of the generalization of threshold dynamics to arbitrary surface tensions given in [EO15]. Its benefits include its unconditional stability (time step size δt can be chosen arbitrarily large, constrained only by accuracy considerations), seamless handling of topological changes in any dimension and very low per time step cost $\mathcal{O}(N \log N)$ on a uniform grid of N points, using the FFT to compute the convolutions. Yet, despite its extreme simplicity, it handles automatically and correctly all the essential features of the dynamics, including Herring angle conditions (6) along junctions, and countless types of topological changes that may occur during the evolution. Note that Algorithm 1 can be seen as a type of level set method, where the function

$$-\psi_i^n(x) + \min_{j \neq i} \psi_j^n(x)$$

plays the role of the level set function depicting the shape of the i -th grain at the $(n+1)$ -th time step. It turns out that this very simple algorithm results in a misorientation dependent mobility $\mu_{i,j}$, associated with the boundary $\Gamma_{i,j}$ between grains i and j that is given by

$$\mu_{i,j} = \frac{1}{\sigma_{i,j}}$$

leading to the normal speed

$$v_{i,j} = \mu_{i,j} \sigma_{i,j} \kappa_{i,j}(x) = \kappa_{i,j}(x)$$

at any point $x \in \Gamma_{i,j}$. In other words, using the Gaussian as the convolution kernel, Algorithm 1 naturally prefers equal (isotropic) *reduced mobilities*: Each interface in the network moves with the same (equal) multiple of its (mean) curvature, and the only difference from the isotropic model are the junction angles.

A more general algorithm was in fact given in [EO15] that allows arbitrary choice of surface tensions *and* mobilities, but is considerably more complicated and deviates from the simplicity of Algorithm 1. In this paper, we use for the first time on large scale simulations a more recent version, namely Algorithm 2, that was proposed in [SE18]. It is simpler and closer in spirit to Algorithm 1 while allowing for both arbitrary surface tensions and arbitrary mobilities. This is achieved by merely replacing the convolution kernel used in Algorithm 1 by the positive sum of two distinct Gaussians, thus preserving the efficiency and simplicity of the original version. As shown in [SE18], in the special but important and very common case of *equal mobilities* (i.e., $\mu_{i,j} = 1$ for all $i \neq j$), a careful choice of the widths of the two Gaussians, denoted by the parameters α and β in what follows, guarantees the

Algorithm 1 (in [EO15])

Given the initial grain shapes $\Sigma_1^0, \dots, \Sigma_N^0$ and a time step size δt , obtain the grain shapes $\Sigma_1^{n+1}, \dots, \Sigma_N^{n+1}$ at the $(n+1)$ -th time from the grain shapes $\Sigma_1^n, \dots, \Sigma_N^n$ at the end of the n -th times as follows:

- (i) Compute the convolutions:

$$\phi_i^n = G_{\sqrt{\delta t}} * \mathbf{1}_{\Sigma_i^n}.$$

- (ii) Form the comparison functions:

$$\psi_i^n = \sum_{j \neq i} \sigma_{i,j} \phi_j^n.$$

- (iii) Update the grain shapes:

$$\Sigma_i^{n+1} = \left\{ x : \psi_i^n(x) < \min_{j \neq i} \psi_j^n(x) \right\}.$$

retention of the major benefits of the original Algorithm 1, namely unconditional stability and convergence to the correct Mullins' energy (1), while allowing its extension to e.g. Read-Shockley surface tensions (2).

Algorithm 2

Given the initial grain shapes $\Sigma_1^0, \dots, \Sigma_N^0$ and a time step size δt , obtain the grain shapes $\Sigma_1^{n+1}, \dots, \Sigma_N^{n+1}$ at the $(n+1)$ -th time from the grain shapes $\Sigma_1^n, \dots, \Sigma_N^n$ at the end of the n -th times as follows:

- (i) Compute the convolutions:

$$\phi_{1,i}^n = G_{\sqrt{\alpha \delta t}} * \mathbf{1}_{\Sigma_i^n} \text{ and } \phi_{2,i}^n = G_{\sqrt{\beta \delta t}} * \mathbf{1}_{\Sigma_i^n}.$$

- (ii) Form the comparison functions:

$$\psi_i^n = \sum_{j \neq i} a_{i,j} \phi_{1,j}^n + b_{i,j} \phi_{2,j}^n$$

where $a_{i,j}$ and $b_{i,j}$ are given by

$$a_{i,j} = \frac{\sqrt{\pi} \sqrt{\alpha}}{\alpha - \beta} (\sigma_{i,j} - \beta \mu_{i,j}^{-1}) \quad \text{and} \quad b_{i,j} = \frac{\sqrt{\pi} \sqrt{\beta}}{\alpha - \beta} (-\sigma_{i,j} + \alpha \mu_{i,j}^{-1}).$$

- (iii) Update the grain shapes:

$$\Sigma_i^{n+1} = \left\{ x : \psi_i^n(x) < \min_{j \neq i} \psi_j^n(x) \right\}.$$

4. LARGE SCALE SIMULATIONS

In this section, we use Algorithms 1 and 2 to study the evolution of large networks of grains, in both 2D and 3D. The 2D simulations are initialized with approximately 100,000 well-resolved grains and are repeated 3 times, while the 3D simulations are initialized with 10,000 grains and repeated 10 times. Recall from the Introduction the following surface tension and mobility models that will be explored in both cases:

- (i) Read-Shockley surface tensions with constant (isotropic) mobilities: $\sigma_{i,j}$ given by (2) and $\mu_{i,j} = 1$.
- (ii) Read-Shockley surface tensions and reciprocal mobilities: $\sigma_{i,j}$ given by (2) and $\mu_{i,j} = \sigma_{i,j}^{-1}$. This results in equal (isotropic) *reduced mobilities*.
- (iii) Equal (isotropic) surface tensions and mobilities: $\sigma_{i,j} = \mu_{i,j} = 1$. This also results in equal (isotropic) reduced mobilities.

Whenever Read-Shockley surface tensions are used, we take the Brandon angle θ_* in (2) to be $\theta_* = 30^\circ$ to agree with simulations performed in Refs. [GMH⁺09, HHM01] and to lie within the experimentally observed range [SB95].

In all simulations, the initial grain configuration is taken to be the Voronoi diagram of a set of points chosen uniformly at random from a periodic box.

4.1. Two spatial dimensions. In these 2D simulations, the initial grain configuration of around 100,000 well-resolved grains is assigned a random fiber texture: All grain orientations are obtained from a reference configuration by a rotation about the axis normal to the 2D domain, and the angle of the rotation is taken from $[0, 2\pi)$ uniformly at random. We present results at two distinct times for each model: model (i) at $t_i = 1.907 \times 10^{-5}$ and $t_f = 8.345 \times 10^{-5}$, model (ii) at $t_i = 1.550 \times 10^{-5}$ and $t_f = 6.259 \times 10^{-5}$ and model (iii) at $t_i = 1.788 \times 10^{-5}$ and $t_f = 7.033 \times 10^{-5}$. The different stopping times ensure that at the intermediate time t_i , around 30% of all grains remain in each one of our runs, while at the final time t_f around 10% of all grains remain. The simulations are performed on a 4096×4096 grid discretizing $[0, 1]^2$.

Algorithm 2 requires choosing the parameters α and β , the widths of the two Gaussian kernels. They need to satisfy

$$\alpha > \max_{i \neq j} \sigma_{ij} \quad \text{and} \quad \beta < \min_{i \neq j} \sigma_{ij}$$

to guarantee the properties described in section 3. However, from a practical point of view, we also need the quotient α/β to remain moderate for accuracy considerations so that the Gaussians have comparable widths and thus may be sampled well without requiring unduly high spatial resolution. Since both α and β depend on the surface tensions which in turn depend on the misorientation angle, this can be accomplished by imposing a minimum misorientation angle between any two grains to be 1° . This reduces the effective size of the surface tension matrix, while keeping the same number of distinct grains, and ultimately results in a small quotient α/β .

We achieve this in the following way. Once the grain orientations are assigned, we partition the domain $[0, 2\pi)$ into equally spaced bins of 1° length. Then all grains with orientations in the same bin are reassigned a new grain orientation, the midpoint of the bin. This is equivalent to assigning grain orientations from the uniform distribution on $\{0.5^\circ, 1.5^\circ, \dots, 359.5^\circ\}$.

Figure 3 shows the time evolution of the GSD for the three different models, while Figure 4 shows the corresponding distributions of reduced effective radii. For models (i) & (ii) with Read-Shockley surface tensions, the distributions appear stationary with no significant difference between the two. The distributions for the isotropic model (iii) are also very similar, except at final time t_f , we see some evidence of the two distinct peaks observed previously in simulations of [MLMS15] with the same isotropic model, but using the very different algorithm of front tracking. This two peak distribution has not been observed in other recent 2D simulations

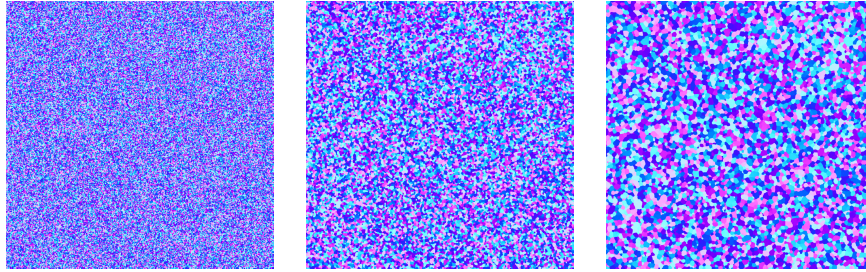


FIGURE 1. The initial microstructure contains 99,130 grains (left). At the intermediate time $t_i = 1.907 \times 10^{-5}$, 29,841 grains remain in full microstructure while at the final time $t_f = 8.345 \times 10^{-5}$, 10,003 grains remain (right). These microstructures were obtained with model (i).

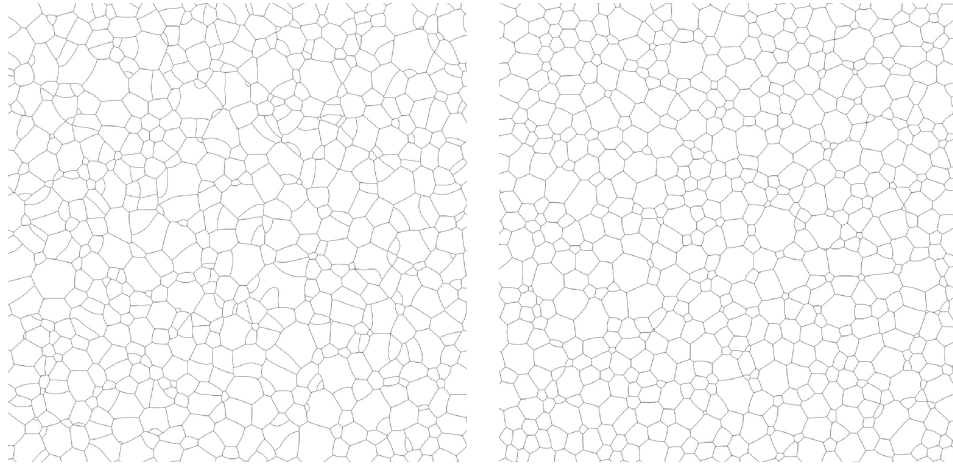


FIGURE 2. Close up of the final microstructures for model (i) (left) and model (iii) (right). The former produces more elongated grains with narrow shapes, while the latter more rounded grains.

of the *isotropic* (constant) surface tension and mobility model (i) in e.g. [KLT06, KKKP06, MTO⁺18], whose results look closer to the ones we obtained with Read-Shockley surface tensions. On the other hand, the recent study [MT17], which includes simulations with models (i) & (iii), also has some evidence of the double peak with model (iii); our results are in close agreement with theirs for both of these models.

The similarity in the GSDs of the three surface tension / mobility models considered here notwithstanding, it is natural to expect some differences when we move on to statistics of grain *shapes*. After all, it is well known that the microstructure of anisotropic models can be visually quite different than that of the isotropic model (see Figures 1 and 2). Indeed, the similarities finally cease when we look at the isoperimetric ratio, also called circularity, which is given by $\frac{4\pi A}{P^2}$ where A and P denote the area and perimeter of the grain, respectively. Figure 5 shows that

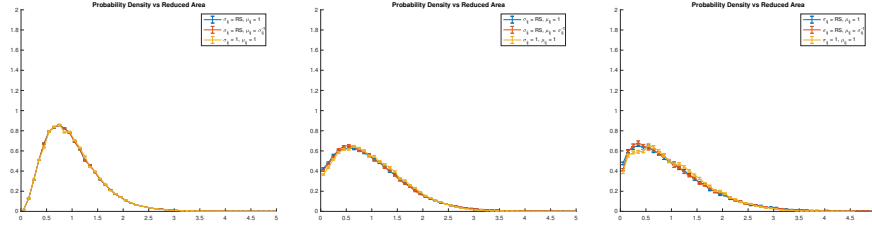


FIGURE 3. GSD (probability density vs. reduced area $\frac{A}{\langle A \rangle}$) for the three different models: initial Voronoi data (left), at time t_i when approximately 30% of grains remain (center) and at time t_f when approximately 10% of grains remains (right).

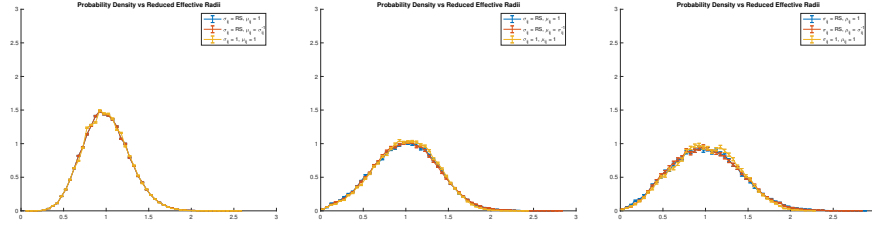


FIGURE 4. Probability density vs. reduced effective radii $\frac{\sqrt{A}}{\sqrt{\langle A \rangle}}$ for the three different models: initial Voronoi data (left), at time t_i when approximately 30% of grains remain (center) and at time t_f when approximately 10% of grains remains (right).

all three surface tension / mobility models lead to peak distributions but with a higher amplitude for the isotropic model. From time t_i to time t_f , while 20,000 disappear, the isoperimetric ratio retains its peaked distribution but with the peak moving towards 1 which indicates that the grains become more rounded.

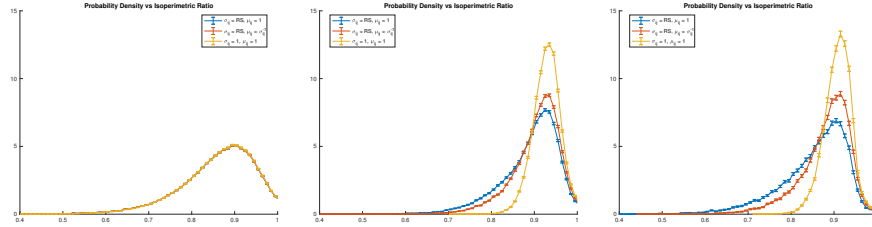


FIGURE 5. Probability density vs isoperimetric ratio $\frac{4\pi A}{L^2}$ for the three different models: initial Voronoi data (left), at time t_i when approximately 30% of grains remain (center) and at time t_f when approximately 10% of grains remains (right).

Finally, Figure 6 shows the MDF for the two unequal surface tension models: Read-Shockley with equal and reciprocal mobilities. Due to its random fiber texture, the MDF of the initial data is uniform. As time evolves, it concentrates at

small misorientations corresponding to small surface tensions. This is in agreement with previous studies, e.g. [HHM01, HMH01, KLR⁺04, EES13]. There is a slight but noticeable difference between the MDFs of the two models, which may in any case keep concentrating at the origin with further evolution: Model (i) has a more concentrated MDF compared to (ii), perhaps because low angle boundaries move slower in model (i) and hence persist longer.

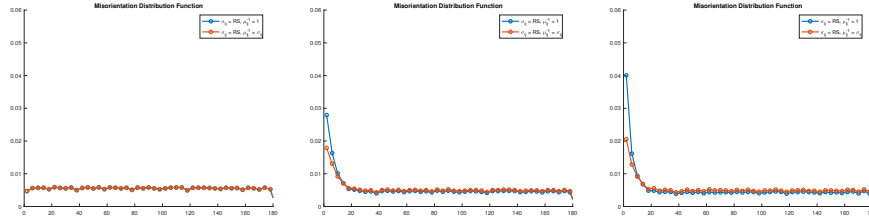


FIGURE 6. Misorientation distribution for models (i) and (ii): initial Voronoi data (left), at time t_i when approximately 30% of grains remain (center) and at time t_f when approximately 10% of grains remains (right).

4.2. Three spatial dimensions. For the 3D simulations, we initialize the microstructure with approximately 10,000 well-resolved grains, chosen as the approximate Voronoi diagram to points placed uniformly at random in a periodic box that is discretized into a $256 \times 256 \times 256$ uniform grid. This results in approximately 12 grid points across each grain in every direction at time $t = 0$, which is roughly the same resolution as in our 2D simulations. Each grain is assigned a fully random orientations from $SO(3)$. We present results at two distinct times for each model: model (i) at $t_i = 4.578 \times 10^{-3}$ and $t_f = 7.629 \times 10^{-3}$, model (ii) and (iii) at $t_i = 1.831 \times 10^{-3}$ and $t_f = 4.578 \times 10^{-3}$. Just like in the 2D simulations, the different stopping times ensure that at the intermediate time t_i , around 30% of all grains remain in each one of our runs, while at the final time t_f around 10% of all grains remain. As in our 2D simulations, we impose a minimum misorientation angle, this time of 5° , between the grains once again in order to keep the quotient α/β that appears in our algorithm at a moderate value. Given that the minimum misorientation angle imposed here is larger than usual, a natural question arises: if it were taken to be smaller, would the different statistics change significantly? In order to investigate this, we run our simulations for model (ii) without doing any merging and observed that the statistics remained essentially the same.

Unlike in our 2D simulations, we see substantial differences in the eventual GSD reached by surface tension / mobility model (i) vs. models (ii) & (iii). Figures 8 and Figure 9 show the time evolution of the GSD in terms of the reduced volume and corresponding effective radii distributions, respectively. We note that while the effective radii distributions of (ii) & (iii) remain very close to each other throughout the evolution (and agree with previous 3D simulations of the same model via different numerical methods, e.g. [KKKP06, EES10, MTO⁺18, MLMS15]), that of (i) is more spread out, and its peak is shifted in the direction of smaller grains – a difference not seen in the 2D simulations with the same algorithms, and at very similar resolutions. Figure 10 suggests the different eventual GSD

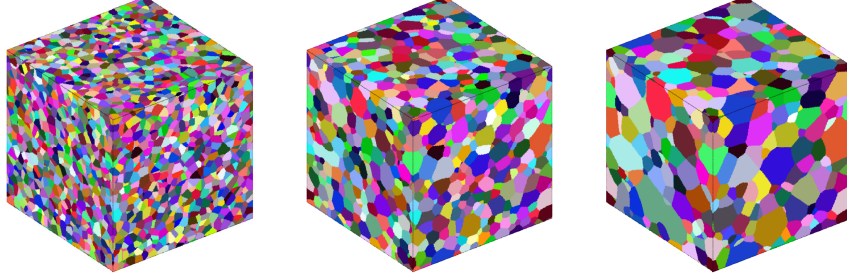


FIGURE 7. The initial microstructure contains 9881 grains (left). At the intermediate time $t_i = 4.578 \times 10^{-3}$, 3031 grains remain in full microstructure while at the final time $t_f = 7.629 \times 10^{-3}$, 998 grains remain (right). These microstructures were obtained with model (i).

observed with surface tension / mobility model (i) may not be inconsistent with experimental data: Two experimental distributions available in existing literature, namely [ZSIE04] and [RLS10], display substantial deviation from the GSD seen in simulations of the isotropic model (iii) in our and previous simulations such as [KKKP06, EES10, MTO⁺18, MLMS15], in the same direction as our simulations with model (i), namely in the direction of smaller grains and more spread out distribution.

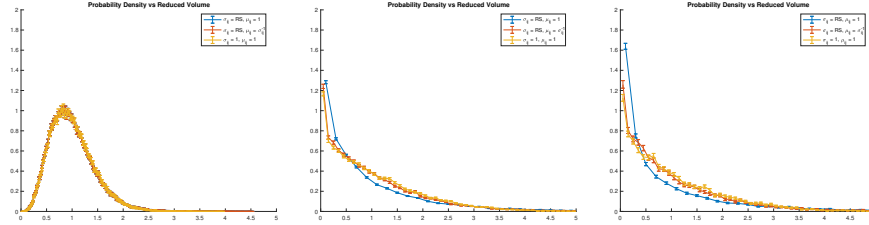


FIGURE 8. GSD (probability density vs. reduced volume $\frac{V}{\langle V \rangle}$) for the three different models: initial Voronoi data (left), at time t_i when approximately 30% of grains remain (center) and at time t_f when approximately 10% of grains remains (right).

Figure 11 shows the distribution of the isoperimetric ratio, namely $\frac{36\pi V^2}{S^3}$, where V denotes the volume and S the surface area of the grain. Remarkably, we see less difference between surface tension / mobility models (ii) and (iii) in 3D than we did in 2D simulations: their stationary isoperimetric ratio distributions are almost identical. The distribution for model (i), however, is broader, indicating a greater presence of eccentric grains compared to the isotropic model (iii), as in our 2D results show in Figure 5.

We now turn to statistics of grain shapes and sizes in 2D slices of 3D data, often called 3DX statistics in the literature. To this end, we took a series of cross sections parallel to the faces of the cubic computational domain $[0, 1]^3$. They were spaced roughly five average grain diameters apart to reduce correlations between

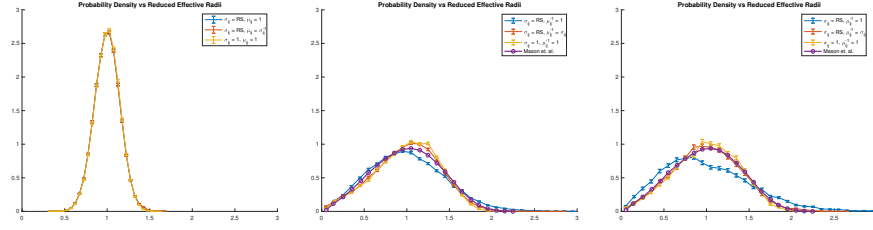


FIGURE 9. Probability density vs. reduced effective radii $\frac{V^{1/3}}{\langle V^{1/3} \rangle}$ for the three different models: initial Voronoi data (left), at time t_i when approximately 30% of grains remain (center) and at time t_f when approximately 10% of grains remains (right).

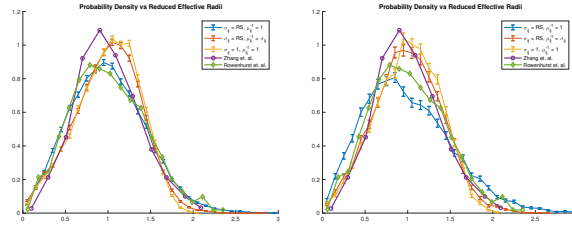


FIGURE 10. Comparison of the GSD in terms of the reduced effective radii distributions in models (i), (ii) and (iii) at time t_i when approximately 30% of grains remain (left) and time t_f when approximately 10% of grains remain (right) with the experimental data from [ZSIE04] and [RLS10].

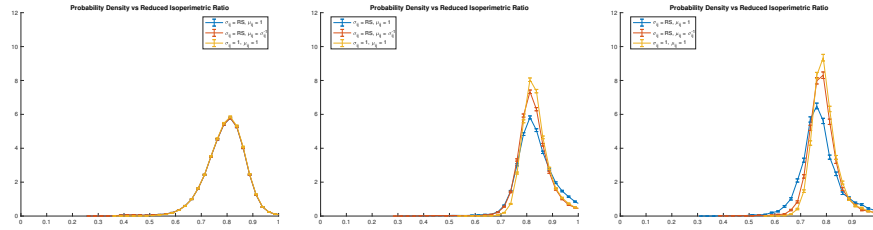


FIGURE 11. Probability Density vs. Isoperimetric Ratio $\frac{36\pi V^2}{S^3}$ for the three different models: initial Voronoi data (left), at time t_i when approximately 30% of grains remain (center) and at time t_f when approximately 10% of grains remains (right).

neighboring cross sections. Figure 12 shows the distribution of GSD in terms of the reduced effective radii distributions. The results are similar to the fully 3D grains: the surface tension / mobility models (ii) and (iii) are close to each other, while the distribution for model (i) is more spread out and its peak is achieved at smaller grains. In Figure 13 we compare the distribution of the isoperimetric ratio, namely $\frac{4\pi A}{P^2}$, where A denotes the area and P the perimeter of the grain in the 2D slice.

All surface tension / mobility models present almost identical peak distributions, with models (ii) and (iii) attaining a higher peak.

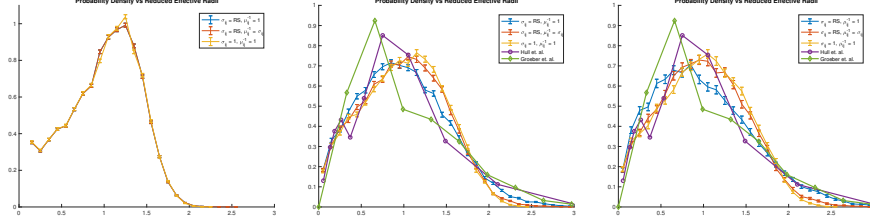


FIGURE 12. Probability density vs reduced effective radii distributions $\frac{\sqrt{A}}{\sqrt{\langle A \rangle}}$ taken from the cross-sections of constant z -value from the initial Voronoi data (left), at time t_i when approximately 30% of grains remain (center) and t_f when approximately 10% of grains remain (right). Experimental data from [Hul88] and [GHU⁺06] is included for comparison.

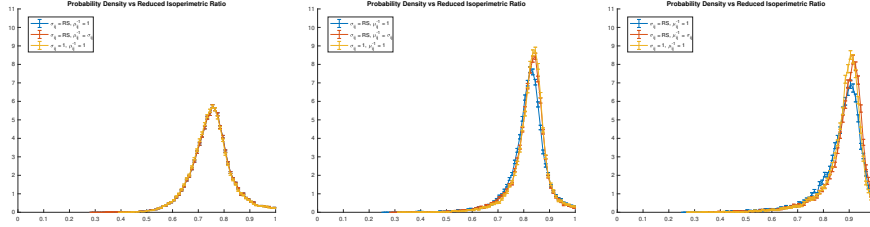


FIGURE 13. Probability density vs isoperimetric ratio $\frac{4\pi A}{L^2}$ taken from the cross-sections of constant z -value from the initial Voronoi data (left), at time t_i when approximately 30% of grains remain (center) and t_f when approximately 10% of grains remain (right).

Finally, we report asymptotic behavior of the MDF in our 3D simulations with surface tension / mobility models (i) & (ii). When the initial data is generated by assigning orientations at random sampled from the uniform distribution on $SO(3)$ to grains from a Voronoi construction, it is well known that the initial MDF is given by the Mackenzie distribution [Mac58]. With this initial data, both models (i) & (ii) behave very similarly: Their MDFs stay in close vicinity of the Mackenzie distribution; see the first row of plots in Figure 14. This observed behavior is in close agreement with previous simulation results, e.g. [HMH01, HMH01, GMH⁺09]. The very slight deviation from the Mackenzie distribution (observed in these previous studies as well) appears to be present mainly in model (ii), and not so much in (i).

We also explore the asymptotic behavior of the MDF when the initial configuration deviates substantially from the Mackenzie distribution. To that end, we devised and implemented an algorithm to modify the randomly assigned initial orientations so that the initial MDF is perturbed substantially away from the Mackenzie distribution. We leave the shapes of the initial grains unchanged, as the random Voronoi

diagram. To be specific, consider the function

$$\text{MDF}_\delta(x) = \sum_{i < j} \text{Area}(\Gamma_{ij}) b_\delta(x - \theta_{ij})$$

for $\delta > 0$ with

$$b_\delta(x) = \frac{1}{\delta\sqrt{2\pi}} e^{-\frac{x^2}{2\delta^2}}.$$

Without loss of generality assume that

$$\sum_{i < j} \text{Area}(\Gamma_{ij}) = 1.$$

Then MDF_δ is a regularized approximation of the MDF of the grain network. Let $T(x)$ denote the desired initial MDF. Based on (4), MDF_δ can be treated as a function of $g_1, \dots, g_N \in SO(3)$, the orientations of each grain, by expressing the misorientation angles θ_{ij} in terms of these. We apply a steepest descent procedure on the L^2 norm of the difference between MDF_δ and T with respect to the orientations g_i of the grains; this updates the initial orientations g_j until the initial MDF closely matches the desired distribution $T(x)$. As this procedure has no preference for a particular orientation, we expect that the initial orientation distribution remains uniform. In other words, our approach allows perturbing the MDF without introducing texture.

The second and third rows of Figure 14 show the evolution of the MDF when it is initially perturbed away from the Mackenzie distribution by this procedure, by two different sized (and quite large) perturbations. In each case, the MDF evolves back to a very close vicinity of the Mackenzie distribution, which is quite different from earlier results in [GMH⁺09], where no steady state MDF is observed in simulations with initial data whose MDFs differ from the Mackenzie distribution. We expect the difference is due to the different ways of generating non-Mackenzie initial data: The method of [GMH⁺09] introduces texture (non-uniform orientation distribution), while ours does not. This is illustrated in Figure 15 where we plot the orientation angle distribution. Here, by orientation angle of a grain we mean its misorientation angle when measured against the sample reference grain, the one that is completely aligned with the axes. In the presence of a random texture the orientation angle distribution will match the Mackenzie distribution.

5. CONCLUSIONS

We investigated, via large scale simulations, the role that surface tension and mobility models play in continuum descriptions of grain growth. This was accomplished by applying in the context of very large numbers of grains the new, extremely simple and streamlined threshold dynamics algorithm recently introduced in [SE18] together with the algorithm previously introduced in [EO15] to perform 2D and 3D simulations. Grain statistics, such as the GSD and the MDF, for three distinct choices of surface tension / mobility models were compared to each other and to available experimental data in existing literature. The 2D simulations did not reveal a strong dependence of the GSD on the surface tension / mobility model used. However, in 3D, a clear distinction emerged between the stationary GSDs of the model with anisotropic reduced mobilities and the other two models considered that had isotropic reduced mobilities. The asymptotic behavior of the MDF was also studied, both in 2D and 3D, using 2D and 3D crystallography, respectively.

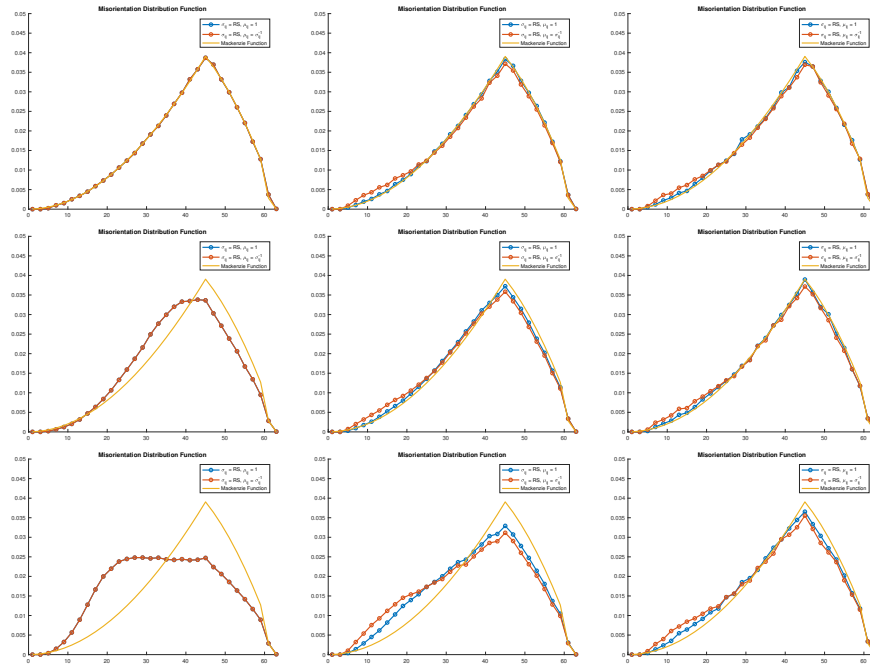


FIGURE 14. Misorientation distribution function for models (i) and (ii) with different initial MDFs at the initial time (left column), at time t_i when approximately 30% of grains remain (middle column) and time t_f when approximately 10% of grains remain (right column).

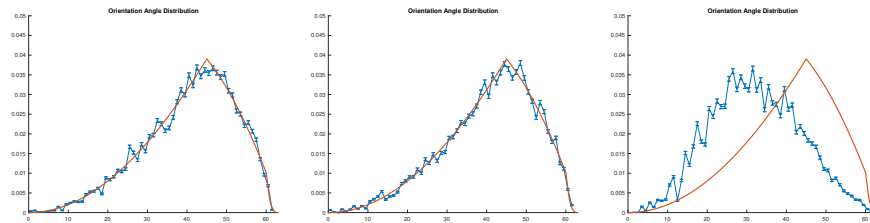


FIGURE 15. Orientation angle distribution (probability density vs orientation angle) for the initial Voronoi data when the MDF is perturbed with the steepest descent procedure described here (left and center graphs whose corresponding MDFs displayed in the second and third row of Figure 14 left column, respectively) and with the method of [GMH+09].

In 3D, it was observed that as long as the orientation texture of the initial data is random, even an initial MDF that is very far from the Mackenzie distribution eventually enters a very close vicinity of it.

6. ACKNOWLEDGEMENTS

The authors gratefully acknowledge support from the NSF grant DMS-1719727.

REFERENCES

- [Bra66] D.G Brandon, *The structure of high-angle grain boundaries*, Acta Metallurgica **14** (1966), no. 11, 1479 – 1484.
- [EES10] Matt Elsey, Selim Esedoğlu, and Peter Smereka, *Large-scale simulation of normal grain growth via diffusion-generated motion*, Proceedings of the Royal Society A: Mathematical, Physical and Engineering Sciences (2010), no. 467.
- [EES13] Matt Elsey, Selim Esedoğlu, and Peter Smereka, *Simulations of anisotropic grain growth: Efficient algorithms and misorientation distributions*, Acta Materialia **61** (2013), no. 6, 2033 – 2043.
- [EO15] Selim Esedoğlu and Felix Otto, *Threshold dynamics for networks with arbitrary surface tensions*, Communications on Pure and Applied Mathematics **68** (2015), no. 5, 808–864.
- [GHU⁺06] M. A. Groeber, B. K. Haley, M. D. Uchic, D. M. Dimiduk, and S. Ghosh, *3D reconstruction and characterization of polycrystalline microstructures using a FIB-SEM system*, Materials Characterization **57** (2006), 259–273.
- [GMH⁺09] J. Gruber, H. M. Miller, T. D. Hoffmann, G. S. Rohrer, and A. D. Rollett, *Misorientation texture development during grain growth. Part I: Simulation and experiment*, Acta Materialia **57** (2009), no. 20, 6102–6112.
- [Hal14] Håkan Hallberg, *Influence of anisotropic grain boundary properties on the evolution of grain boundary character distribution during grain growth—a 2d level set study*, Modelling and Simulation in Materials Science and Engineering **22** (2014), no. 8, 085005.
- [Her99] Conyers Herring, *Surface tension as a motivation for sintering*, pp. 33–69, Springer Berlin Heidelberg, Berlin, Heidelberg, 1999.
- [HHM01] E.A. Holm, G.N. Hassold, and M.A. Miodownik, *On misorientation distribution evolution during anisotropic grain growth*, Acta Materialia **49** (2001), no. 15, 2981 – 2991.
- [HMH01] E.A. Holm, M Miodownik, and G.N. Hassold, *Dimensional effects on anisotropic grain growth*, pp. 239 – 244, Unknown Publisher, 2001 (English).
- [Hul88] F. C. Hull, *Plane section and spatial characteristics of equiaxed β -brass grains*, Materials Science and Technology **4** (1988), no. 9, 778–785.
- [Hum97] F.J. Humphreys, *A unified theory of recovery, recrystallization and grain growth, based on the stability and growth of cellular microstructures—i. the basic model*, Acta Materialia **45** (1997), no. 10, 4231 – 4240.
- [KKKP06] Seong Gyoon Kim, Dong Ik Kim, Won Tae Kim, and Yong Bum Park, *Computer simulations of two-dimensional and three-dimensional ideal grain growth*, Phys. Rev. E **74** (2006), 061605.
- [KLR⁺04] D. Kinderlehrer, Irene Livshits, Gregory S. Rohrer, Shlomo Ta’asan, and Peng Yu, *Mesoscale simulation of the evolution of the grain boundary character distribution*, Recrystallization and Grain Growth, Materials Science Forum, vol. 467, Trans Tech Publications Ltd, 8 2004, pp. 1063–1068.
- [KLT06] David Kinderlehrer, Irene Livshits, and Shlomo Ta’asan, *A variational approach to modeling and simulation of grain growth*, SIAM J. Sci. Comput. **28** (2006), no. 5, 1694–1715.
- [Mac58] J. K. Mackenzie, *Second paper on statistics associated with the random disorientation of cubes*, Biometrika **45** (1958), no. 1/2, 229–240.
- [MBO92] B. Merriman, J. Bence, and S. Osher, *Diffusion generated motion by mean curvature*, The Computational Crystal Growers. AMS Selection in Math. (1992), 73–83.
- [MBO94] Barry Merriman, James K. Bence, and Stanley J. Osher, *Motion of multiple junctions: a level set approach*, J. Comput. Phys. **112** (1994), no. 2, 334–363. MR 1277282
- [MLMS15] Jeremy K. Mason, Emanuel A. Lazar, Robert D. MacPherson, and David J. Srolovitz, *Geometric and topological properties of the canonical grain-growth microstructure*, Phys. Rev. E **92** (2015), 063308.

- [MT17] Eisuke Miyoshi and Tomohiro Takaki, *Multi-phase-field study of the effects of anisotropic grain-boundary properties on polycrystalline grain growth*, Journal of Crystal Growth **474** (2017), 160 – 165, The 8th International Workshop on Modeling in Crystal Growth.
- [MTO⁺17] Eisuke Miyoshi, Tomohiro Takaki, Munekazu Ohno, Yasushi Shibuta, Shinji Sakane, Takashi Shimokawabe, and Takayuki Aoki, *Ultra-large-scale phase-field simulation study of ideal grain growth*, npj Computational Materials **3** (2017), no. 1, 25.
- [MTO⁺18] ———, *Correlation between three-dimensional and cross-sectional characteristics of ideal grain growth: large-scale phase-field simulation study*, Journal of Materials Science **53** (2018), no. 21, 15165–15180.
- [Mul56] W. W. Mullins, *Two-dimensional motion of idealized grain boundaries*, Journal of Applied Physics **27** (1956), no. 8, 900–904.
- [RLS10] D. J. Rowenhurst, A. C. Lewis, and G. Spanos, *Three-dimensional analysis of grain topology and interface curvature in β -titanium alloy*, Acta Materialia **58** (2010), 5511–5519.
- [RS50] W. T. Read and W. Shockley, *Dislocation models of crystal grain boundaries*, Phys. Rev. **78** (1950), 275–289.
- [SB95] A.P. Sutton and R.W. Balluffi, *Interfaces in crystalline materials*, Monographs on the physics and chemistry of materials, Clarendon Press, 1995.
- [SE18] Tiago Salvador and Selim Esedoğlu, *A simplified threshold dynamics algorithm for isotropic surface energies*, Journal of Scientific Computing (2018).
- [UHK⁺02] M. Upmanyu, G. N. Hassold, A. Kazaryan, E. A. Holm, Y. Wang, B. Patton, and D. J. Srolovitz, *Boundary mobility and energy anisotropy effects on microstructural evolution during grain growth*, Interface Science **10** (2002), 201–216.
- [ZS06] D. Zoellner and P. Streitenberger, *Three-dimensional normal grain growth: Monte-Carlo Potts model simulation and analytical mean field theory*, Scripta Materialia **54** (2006), 1697–1702.
- [ZSIE04] C. Zhang, A. Suzuki, T. Ishimaru, and M. Enomoto, *Characterization of three-dimensional grain structure in polycrystalline iron by serial sectioning*, Metallurgical and Materials Transactions A **35A** (2004), 1927–1933.

DEPARTMENT OF MATHEMATICS, MICHIGAN UNIVERSITY, 530 CHURCH ST. ANN ARBOR, MI 48105 (saldanha@umich.edu).

DEPARTMENT OF MATHEMATICS, MICHIGAN UNIVERSITY, 530 CHURCH ST. ANN ARBOR, MI 48105 (esedoglu@umich.edu).